

## VIS-active TiO<sub>2</sub> films decorated by expanded graphite: impact of the exfoliation time on the photocatalytic behaviour

Rodrigo Teixeira Bento, Olandir Vercino Correa, Pedro Lana Gastelois & Marina Fuser Pillis

To cite this article: Rodrigo Teixeira Bento, Olandir Vercino Correa, Pedro Lana Gastelois & Marina Fuser Pillis (2024) VIS-active TiO<sub>2</sub> films decorated by expanded graphite: impact of the exfoliation time on the photocatalytic behaviour, Environmental Technology, 45:10, 2022-2033, DOI: [10.1080/09593330.2022.2163708](https://doi.org/10.1080/09593330.2022.2163708)

To link to this article: <https://doi.org/10.1080/09593330.2022.2163708>



Published online: 11 Jan 2023.



Submit your article to this journal [↗](#)



Article views: 102



View related articles [↗](#)



View Crossmark data [↗](#)



Citing articles: 1 View citing articles [↗](#)



# VIS-active TiO<sub>2</sub> films decorated by expanded graphite: impact of the exfoliation time on the photocatalytic behaviour

Rodrigo Teixeira Bento <sup>a</sup>, Olandir Vercino Correa<sup>a</sup>, Pedro Lana Gastelois<sup>b</sup> and Marina Fuser Pillis<sup>a</sup>

<sup>a</sup>Nuclear and Energy Research Institute, IPEN–CNEN/SP, University of São Paulo, São Paulo, Brazil; <sup>b</sup>Nuclear Technology Development Center, CDTN–CNEN/MG, Federal University of Minas Gerais, Belo Horizonte, Brazil

## ABSTRACT

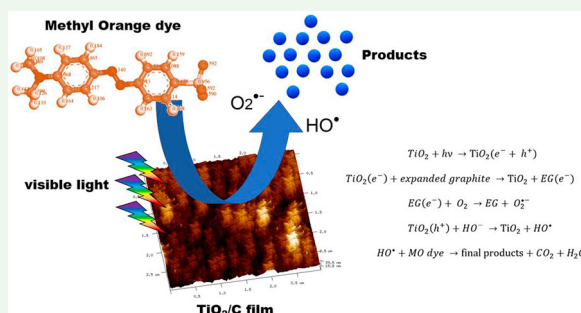
TiO<sub>2</sub>/C nanocomposite films were applied on water treatment. Expanded graphite nanosheets (EG) were obtained by UVC-assisted liquid-phase exfoliation technique, without the addition of acids, surfactants, or aggressive oxidizing agents, which characterizes the process as an eco-friendly method. The carbon nanosheets were synthesized directly from graphite bulk at different times and deposited on TiO<sub>2</sub> films surface by airbrush spray coating method, forming a TiO<sub>2</sub>/C heterojunction. The increase in the exfoliation time promoted a more efficient photocatalytic dye removal under visible light. Morphological modifications, changes in the electronic structure, and wide range of light absorption were observed from the TiO<sub>2</sub>/C heterojunction formation. The results showed that hybrid TiO<sub>2</sub>/C supported photocatalyst is a promise alternative for practical photocatalytic applications under sunlight.

## ARTICLE HISTORY

Received 21 September 2022  
Accepted 20 December 2022

## KEYWORDS

Expanded graphite; TiO<sub>2</sub>; liquid-phase exfoliation; photocatalysis; heterojunction



## Highlights

- Expanded graphite (EG) was obtained at room temperature by an efficient novel green method.
- TiO<sub>2</sub>/C hybrid films were successfully deposited by the facile airbrush spray coating technique.
- Morphological modifications and changes in the electronic structure were observed from the TiO<sub>2</sub>/C heterojunction formation.
- Carbon exfoliation time have great influence on the photocatalytic behaviour of the nanocomposite films.
- TiO<sub>2</sub>/C hybrid film presented 50% of dye removal under visible light.

## 1. Introduction

Water pollution due to improperly disposed organic compounds is currently a major public health concern

[1,2]. Among the main residues that cause pollution of water reserves and springs, pharmaceutical products, pesticides and herbicides, hormones, fats, dyes, and personal care products stand out [3,4]. Conventional water treatments, in addition to using several processing steps, are not able to eliminate such substances. The heterogeneous photocatalysis process is a promising green technology for the removal of many organic and inorganic pollutants from water and air [5,6]. Such a process is characterized by the action of radiation – UV or visible – in the presence of a catalysing material, which absorbs light ( $h\nu$ ) and promotes the chemical transformation of products by oxidation–reduction reactions containing hydroxyl radicals ( $HO^\cdot$ ) generated from water [7].

Among the semiconductor materials most used in photocatalytic processes, titanium dioxide (TiO<sub>2</sub>) has been widely investigated as a promising photocatalyst

in the removal and treatment of organic contaminants from water and air [3,8]. TiO<sub>2</sub> crystalline structure has a great influence on its photocatalytic properties. Anatase and rutile phases present photoactivity [9]. However, the anatase-TiO<sub>2</sub> phase is the most efficient due to the lower rate of recombination of the electron (e<sup>-</sup>)/hole (h<sup>+</sup>) pairs [10].

Nevertheless, the photocatalytic activity of TiO<sub>2</sub> is limited to UV radiation (band gap energy = 3.26 eV for anatase-TiO<sub>2</sub>) [3,11]. Thus, its structural and morphological modification, such as heterojunction formation [12–14], can be a favourable way to increase its efficiency, and allow its use under visible light.

Recent research highlights show that the integration of TiO<sub>2</sub> with graphite, carbon nitride (C<sub>3</sub>N<sub>4</sub>), graphene and other carbonaceous materials can increase the photocatalytic activity of the semiconductor for removing dyes from water, due to the additional carbon properties [15–18].

Recently, expanded graphite (EG), obtained from liquid-phase exfoliation (LPE) techniques, has been investigated as an important modifier for heterostructured semiconductor-carbon photocatalysts. Jia et al. [19] suggested that the incorporation of C atoms into the TiO<sub>2</sub> crystal lattice can be facilitated by the use of graphite, positive replacing graphene, carbon nanotubes, and reduced graphene oxide – commonly used in photocatalytic processes. Jiang et al. [20] observed that the photocatalytic behaviour of hybrids was optimized by the semiconductor-carbon (S–C) heterojunction formation between TiO<sub>2</sub> and graphite, reaching an efficiency of approximately 81% in phenol degradation. Zhang et al. [21] prepared TiO<sub>2</sub>/EG nanosheets photocatalysts by sol–gel method to degrade diesel under visible light, with an efficiency of 88%.

In this paper, we propose the synthesis and characterization of TiO<sub>2</sub> films decorated by expanded graphite nanosheets. The films were applied by a simple cold spray coating method, and the EG was obtained in a single step by UVC-assisted liquid-phase exfoliation method using an aqueous solution of ordinary solvents as acetone and isopropanol. The effects of the exfoliation time on the morphological characteristics, structural properties, and photocatalytic efficiency of the composite films are presented and discussed.

## 2. Methods

### 2.1. Synthesis of expanded graphite

The present method comprises the mechanical milling and sieving steps of the graphite until obtaining a mean particle size less than 38 µm. Nuclear grade

graphite currently employed in nuclear reactors was used as a carbon precursor. The graphite (0.6 g) is dispersed in a solution (60 mL, ratio 1:1:1) containing deionized water, isopropyl alcohol (Dinâmica Química Contemporânea LTDA, C<sub>3</sub>H<sub>8</sub>O, molecular weight 60.1, 99.5%) and acetone (Dinâmica Química Contemporânea LTDA, CH<sub>3</sub>(CO)CH<sub>3</sub>, molecular weight 58.08, 99.5%), under constant agitation with synthetic air (N<sub>2</sub> / 20% O<sub>2</sub>). The dispersion was irradiated with UVC light (λ = 253.7 nm, OSRAM Licht AG, Puritec 9W) at room temperature for 2, 8, and 24 h. Lastly, the expanded graphite (EG) was dried in an oven at 50°C for 24 h.

### 2.2. TiO<sub>2</sub> films

300 nm-thick TiO<sub>2</sub> films were obtained by sol–gel method. 5 mL of titanium(IV) isopropoxide (TTiP, Ti(OCH(CH<sub>3</sub>)<sub>2</sub>)<sub>4</sub>, 97%, Sigma-Aldrich) dissolved in 50 mL of isopropanol, and followed by 1.5 mL of sulphuric acid (H<sub>2</sub>SO<sub>4</sub>) adding to control the pH (pH~3). The solution was stirred at 75°C for 60 min. Then, the films were supported on borosilicate glass substrates (25 × 76 × 1 mm) by the versatile and low-cost cold spray coating technique using an airbrush. The speed feed rate was set around 17 mm s<sup>-1</sup>. The samples were dried for 60 min at 100°C, and then calcined at 550°C for 30 min.

### 2.3. TiO<sub>2</sub>/C films

TiO<sub>2</sub> films decorated by EG nanosheets were obtained by spraying the graphite suspension on the TiO<sub>2</sub> layer. The suspension consisted of 0.6 mg of EG in 60 mL of isopropanol and was sonicated for 10 min before being applied on the top the TiO<sub>2</sub> film at room temperature. The influence of graphite exfoliation time on the visible-light photocatalytic efficiency was evaluated. After spraying the EG on the TiO<sub>2</sub> films surface, the nanocomposite photocatalysts were dried at 100°C for 60 min.

### 2.4. Characterization

The morphological, structural, chemical, and thermal characteristics of the samples were evaluated by scanning electron microscopy (FE-SEM, JEOL JSM-6701F), Raman spectroscopy (WITEC Raman Microscope Alpha300 R, λ = 532 nm, 1000–3500 cm<sup>-1</sup>), X-ray diffraction (XRD, Rigaku Multiflex, CuKα radiation, θ2θ mode), Fourier Transform infrared spectra (FT-IR, Nicolet spectrometer, frequency range of 3000 cm<sup>-1</sup>–600 cm<sup>-1</sup> at room temperature), and atomic force microscopy (AFM, SPM Bruker NanoScope IIIA, scan frequency of

0.601 Hz, scan size of  $3 \times 3 \mu\text{m}$ ). X-ray photoelectron spectroscopy (XPS) experiments were conducted on a SPECS system (SPECS, Berlin, Germany) equipped with a PHOIBOS 150 MCD analyzer, and a monochromatic Al K $\alpha$  X-ray radiation source of 1486.6 eV. The survey spectra were acquired using pass energy of 100 eV and an energy step of 1 eV. The high-resolution spectra were acquired using pass energy of 20 eV and an energy step of 0.1 eV. The experimental data were fitted with CasaXPS software using a combination of Gaussian/Lorentzian curves on a Shirley background. The UV-Vis absorption spectra of the TiO<sub>2</sub> and TiO<sub>2</sub>/C films were obtained using a Shimadzu UV-Vis spectrophotometer equipment, model UV-1650PC, in the range of  $300 \text{ nm} \leq \lambda \leq 1100 \text{ nm}$ , with a step of 1 nm. The band gap energy values of the samples were estimated using the Tauc method (Equation (1)) [22]:

$$(\alpha \cdot h\nu)^{\frac{1}{n}} = B(h\nu - E_g) \quad (1)$$

where  $h$  is Planck's constant;  $\nu$  is the photon frequency;  $B$  is a constant; and  $E_g$  is the band gap energy. The  $1/n$  factor depends on the nature of the electron transition and is equal to 1/2 for direct transition band gaps, as in the case of TiO<sub>2</sub>, and 2 for indirect transition band gaps [22].

## 2.5. Photocatalytic experiments

Photocatalytic behaviour of the TiO<sub>2</sub>/C hybrid films was evaluated by the methyl orange dye (MO) decolorization under visible light irradiation (Royal Philips Electronics; four tubular LED lamps with 3 W each;  $\lambda = 400\sim 700 \text{ nm}$ ). Each test consisted of 5 h under controlled temperature (19–20°C). The experiments were carried out in a homemade photocatalytic reactor setup previously described [5,9]. MO dye was used as pollutant model ( $0.005 \text{ g L}^{-1}$ ), at pH = 2, and volume of 40 mL. All films and dye solution remained in the dark for one hour to achieve the adsorption-desorption equilibrium of the dye molecules on the photocatalyst surface. Dye removal changes were investigated by UV-Vis spectroscopy (Global Trade Technology,  $\lambda = 464 \text{ nm}$ ), and the measurements were taken every 30 min. The photocatalytic parameters were defined according to previous works [7,23,24].

The apparent rate constant ( $k_{ap}$ ) was estimated from the  $\ln(C_0/C)$  graph, in order to evaluate the methyl orange dye removal rate from exposure to photocatalysts as a function of time, assuming a reaction pseudo-first order, according to the model proposed by Langmuir Hinshelwood [7,23] (Equation (2)), in

which  $k_{ap}$  is the apparent rate constant,  $t$  is the time,  $C_0$  is the initial concentration of the dye, and  $C$  is the concentration in each time instant:

$$\ln(C_0/C) = k_{ap}t \quad (2)$$

## 3. Results and discussion

### 3.1. Characterization of expanded graphite nanosheets

#### 3.1.1. Morphological evaluation

From Figure 1(a) it can be observed that graphite flakes are thick and formed by compacted sheets with mean size of  $6.5 \mu\text{m}$ , and thickness of  $2.7 \mu\text{m}$  approximately. After the liquid-phase exfoliation the samples exhibited some spaced layers of carbon (Figure 2(b–d)), in the form of nanosheets that show mean thickness values around 5.95 and 1.68 nm, respectively, for the samples obtained between 2 and 24 h.

The liquid-phase exfoliation (LPE) technique is a simple method that allows to get few defects graphite nanosheets at room temperature, and without using acids or oxidizing agents as in conventional techniques, so the formation of hazardous toxic waste, and damage to environment and human health are avoided [25].

In the LPE process, the graphite layers were exfoliated by breaking the van der Waals bonds [26,27]. The UVC-assisted LPE mechanisms of graphite are still little discussed. However, based on the results obtained and data presented in the literature [28,29] it can be considered that a hydrolysis reaction of the solution occurs during the UVC irradiation. This process promotes the formation of  $\text{H}^+$  and  $\text{HO}^-$  ions, hydrated electrons ( $e_{aq}^-$ ) and new oxidizing compounds [29]. The  $e_{aq}^-$  are the dominant species in the reduction stage, with high reducing potential ( $E_0 = 2.67 \text{ V}$ ) [30]. The increase in the entropy of the system induces an exothermic reaction that releases a large amount of energy capable of fragmenting the graphite structure, and consequently promote the liquid-phase exfoliation.

#### 3.1.2. Chemical structure

FT-IR analysis was performed to characterize the functional groups present on the carbon chemical structure (Figure 2(a)). Graphite clean spectrum did not show any significant peak, however presented three low-intensity bands at 2372, 2046, and  $1975 \text{ cm}^{-1}$ . The observed few absorption signals can be associated to the graphite chemical inertness, and to the different charge states of the C=C bonds [31,32]. After the UVC-assisted LPE process, peaks of oxygenated functional

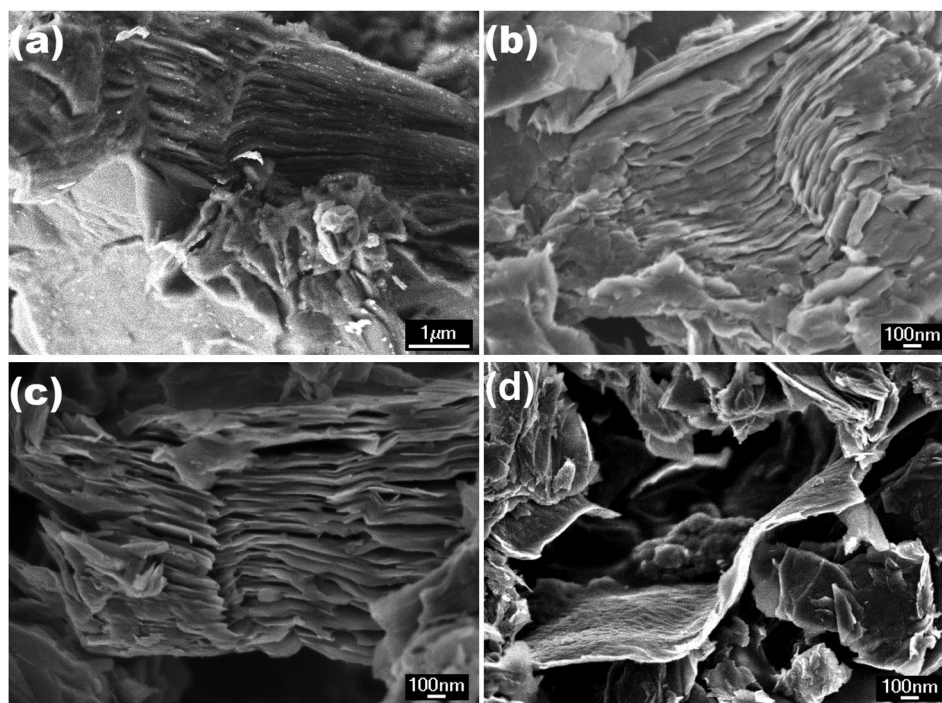


**Figure 1.** FE-SEM images of (a) bulk graphite, and expanded graphite (EG) obtained by UVC-assisted liquid-phase exfoliation (LPE) technique at room temperature for (b) 2 h, (c) 8 h, and (d) 24 h.

groups appeared, which suggests the partial formation of oxygen functional groups. The EG exhibited a long absorption band in the  $600\text{--}900\text{ cm}^{-1}$  range. The bands at  $2158$ ,  $2930$ , and  $2855\text{ cm}^{-1}$  correspond, respectively, to the symmetric and asymmetric stretching vibration of C-H bond in  $\text{sp}^3$ -bonded carbon network [32–34]. The very weak band at  $2372\text{ cm}^{-1}$  is related to  $\text{CO}_2$  residual molecules formed during the process [35,36]. An absorption peak at  $1726\text{ cm}^{-1}$  is related to the  $n\text{--}\pi^*$  transition of the carbonyl group (C=O stretching vibration) [32,33]. The bands observed

at  $1624$ ,  $1574$ , and  $1557\text{ cm}^{-1}$  correspond to aromatic C=C bonds, associated to the stretch mode of characteristic  $\text{sp}^2$  hybridization, and can be attributed to  $\pi\text{--}\pi^*$  transition [31,32]. O-H was identified at  $1410\text{ cm}^{-1}$ . The two peaks around  $1026$  and  $671\text{ cm}^{-1}$  refer to the C-O and C-OH stretching vibrations of oxygen functional groups [31,32,34].

The FT-IR results showed that the intensity of the graphite absorption bands increases significantly with its oxidation, followed by a reduction on the peaks intensity with the increasing of UVC exposure time, which

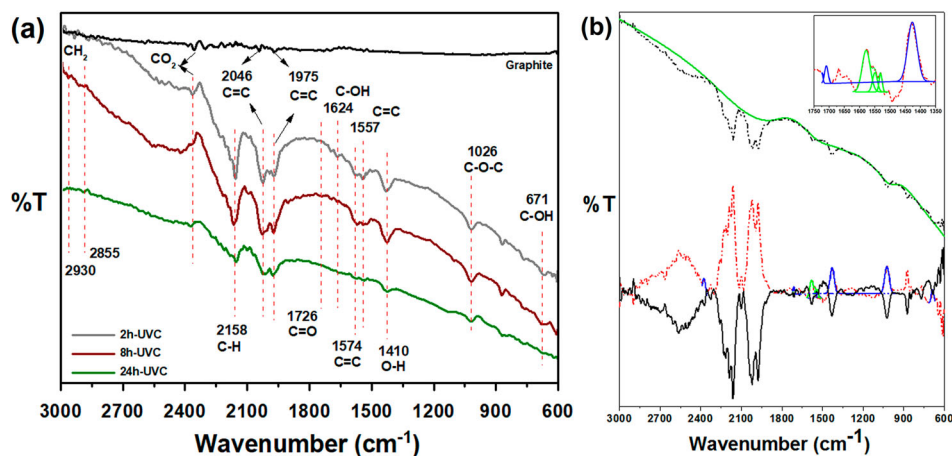


**Figure 2.** (a) FT-IR spectra of the bulk and expanded graphite synthesized by UVC-assisted liquid-phase exfoliation method; (b) Details of the FT-IR spectra treatment from the exfoliated samples and deconvolution to obtain the ORB:total ratio areas for quantification.

**Table 1.** Surface elemental quantitative analyses of expanded graphite nanosheets: C 1s region, O 1s region, O/C ratio, and ORB:total ratio summary results from XPS and FT-IR.

	Elemental composition (at%)		C1s peak deconvolution (%)					C:O ratio	ORB: total ratio
	O	C	C–C	C–O	O–C=O	C=O	$\pi$ - $\pi$		
<b>Graphite</b>	17.3	72.0	85.5	2.3	2.5	7.6	2.1	4.16	–
<b>EG 2h</b>	3.7	96.3	97.9	0.9	0.7	–	0.5	26.03	0.75
<b>EG 8h</b>	3.0	97.0	94.4	1.6	1.1	–	2.9	32.33	0.57
<b>EG 24h</b>	2.4	97.6	95.2	1.3	0.9	–	2.6	40.67	0.31

suggest that the samples were highly reduced as the UVC exposition time arises. The results corroborate the FE-SEM images, and suggest the efficiency in the process of the layers separation and subsequent reduction of the functional groups [27,30].

Figure 2(b) exhibits the FT-IR quantitative analysis of the EG sample to estimate the oxygen related bands ratio (ORB:total ratio), according to Equation (3) [37]. Firstly, the baseline spectrum was subtracted from the original FT-IR data of all samples. The resulting spectra was multiplied by  $-1$ , and then all oxygen related bands were deconvoluted into Gaussian peaks to obtain its areas ( $A_{total}$ ). The  $1557\text{ cm}^{-1}$  peak (aromatic C=C bonds) was also deconvoluted ( $A_{C=C}$ ). The calculation method allows to evaluate the functionalization degree of the nanosheets.

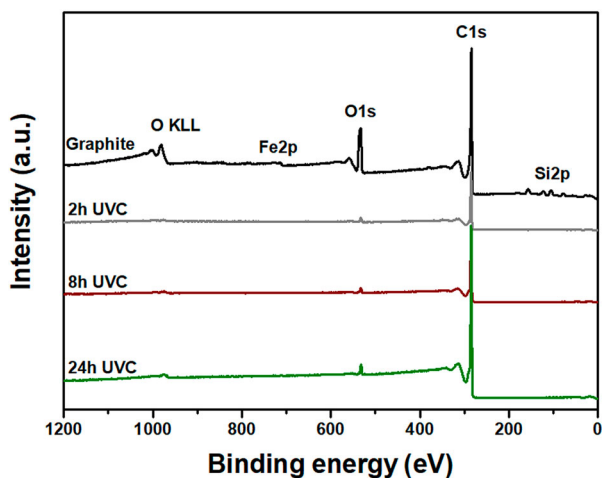
$$\text{ORB:total ratio} = \frac{A_{total} - A_{C=C}}{A_{total}} \quad (3)$$

ORB:total ratios values between 0.3 and 0.7 were found (Table 1). Previous research demonstrated a similar trend [37,38]. The results suggested the effect of the preparation conditions on the ORB:total ratio variation. The residence time under UVC radiation largely influences the molecular structure of the expanded graphite

nanosheets. Increasing the UVC time, there was a reduction in the O/C ratio present in the samples. The present results are satisfactory, nevertheless further detailed studies will be conducted to assess the concentration variations effects.

The chemical state in EG samples, its functional groups, and the C:O (carbon to oxygen) atomic ratio have been investigated by XPS, as shown in survey scans (Figure 3). Peaks of C and O were found in all samples. The bulk graphite also presented peaks of Si (5.6 at%), Al (4.9 at%), and Fe (0.2 at%) – possibly as contamination from the mechanical milling process, before the sieving step. After the liquid-phase exfoliation process under UVC irradiation, a higher C:O ratio is observed, and as consequence a lower number of oxygenated groups (Table 1). After 2 h of treatment, the O content decreased from 17.3% to 3.7%, and after 24 h of UVC irradiation the maximum C:O ratio around 40.7 was achieved. The respective behaviour corroborates the FT-IR results for the ORB: total ratio, suggesting a removal of the oxygenated groups.

The high-resolution C1s XPS core-level spectra have also been realized (Figure 4). In the C1s region, peaks attributed to C–C/C=C (284.6 eV), C–O (286.4 eV), COOH (289.1 eV) groups, and  $\pi$ - $\pi$  (290.9 eV) bonding were clearly founded in all samples [29,37], which was also identified by the FT-IR signals. The bulk graphite spectra (Figure 4(a)) showed an additional peak at 287.5 eV, corresponding to C=O bonding. The contribution of C–C bonding (carbon with  $sp^2$  hybridization) [39], to the total C1s signal was about 85% for graphite, and increased to 98%, approximately, after 2 h of UVC irradiation (Figure 4(b)), until it stabilizes around 95% with increasing the process time (Figure 4(c–d)). This behaviour suggests that the  $sp^2$  domains into the structural network was partially restored after the liquid-exfoliation process [27,40], which corroborates the XRD and Raman results. After the UVC irradiation process, it was notably observed that the C=O bonding disappears from the nanosheets, and the COOH intensity enhances. Xue et al. [41] and Tang et al. [42] exhibited similar results. The C=O reduction mechanism can be mainly attributed to reaction between the C=O bonds with hydrogen molecules to yield hydroxyl groups [40,43] –

**Figure 3.** XPS survey spectra of bulk and expanded graphite nanosheets obtained by UVC-assisted liquid-phase exfoliation method irradiated under UVC light at different times.

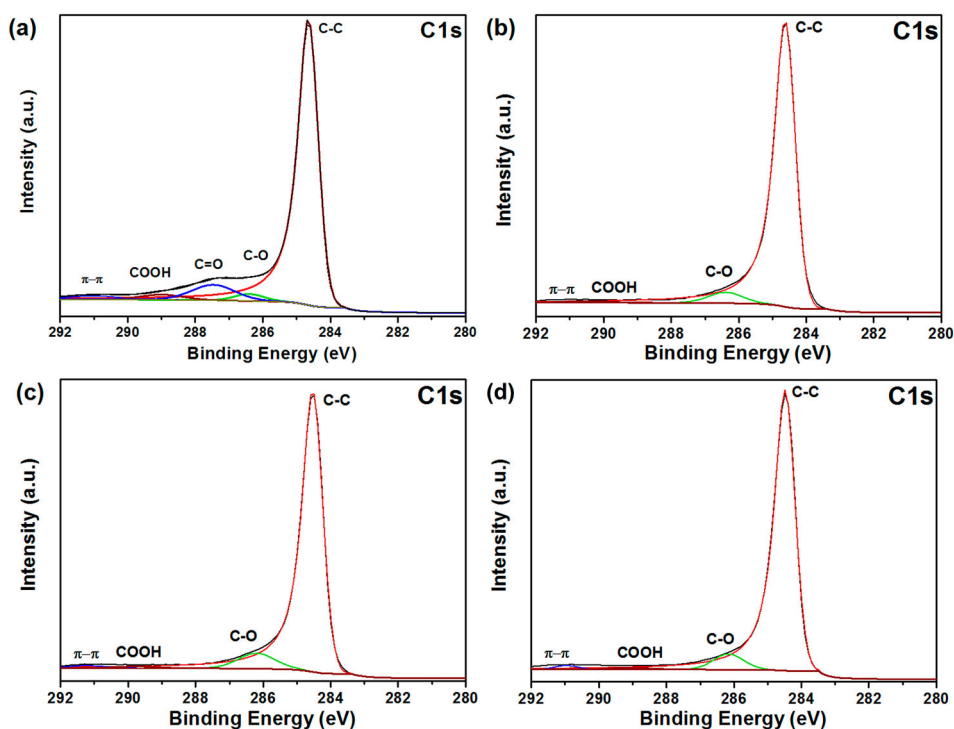


**Figure 4.** C1s core-level XPS spectra of (a) bulk graphite, and expanded graphite samples obtained by UVC-assisted liquid-phase exfoliation method at (b) 2 h, (c) 8 h, and (d) 24 h.

effect that justifies the increase of the COOH amount (Table 1). The decrease in the oxygen-containing groups is indicative of a new reduction mechanism provided by UVC irradiation [40].

### 3.2. Characterization of TiO<sub>2</sub>/C heterojunctions

Anatase-TiO<sub>2</sub> films synthesized by sol-gel technique, deposited on borosilicate glass substrates, and heat treated at 550°C were coated with graphite UVC liquid-phase exfoliated at 2, 8, and 24 h, respectively. Figure 5 presents the AFM images of surface morphology of the pure anatase-TiO<sub>2</sub> film and TiO<sub>2</sub>/C composite films. The anatase-TiO<sub>2</sub> film (Figure 5(a)) shows a homogeneous aspect of the surface, formed by spherical and small grains without visible cracks or pores. On the other hand, when EG is added, the surface is quite modified compared to pure anatase-TiO<sub>2</sub>. The presence of dispersed exfoliated graphite on the film's surface is evident. The TiO<sub>2</sub>/C film decorated by EG nanosheets obtained at 24 h (Figure 5(d)) exhibited the formation of porous and a rough morphology probably resulted from agglomeration. The variation in root mean square (RMS) roughness with the different graphite exfoliation time was not linear due to the heterogeneity of the composites. The surface roughness of anatase-TiO<sub>2</sub> and TiO<sub>2</sub>/C films have increased from, approximately, 12 to 14 and 23 nm, respectively, for EG synthesized at 8 and 24 h. The

composite film coated with EG obtained at 2 h did not show significant changes in the surface height profile.

Figure 6(a) exhibits the Raman spectra of TiO<sub>2</sub>/C films. The Raman spectra of films heat treated at 550°C indicate signal peaks at 144, 197, 397, 515 e 639 cm<sup>-1</sup>, which can be attributed to E<sub>g</sub>, E<sub>g</sub>, B<sub>1g</sub>, A<sub>1g</sub>, or B<sub>2g</sub>, and E<sub>g</sub> vibration modes of anatase-TiO<sub>2</sub> phase, respectively [44,45]. No peaks related to rutile phase or other TiO<sub>2</sub> polymorphs were observed in the films. Figure 6(b) shows the XRD patterns of the TiO<sub>2</sub> and TiO<sub>2</sub>/C films. All films presented good crystallinity, and the XRD spectra suggest the characteristic peaks corresponding to the anatase-TiO<sub>2</sub> crystalline phase (JCPDS 21-1272) [7,17,46]. Graphite peaks between 23°~26° corresponding to (002) crystallographic plane, were also found on the decorated films. No diffraction peaks were observed for other carbon species, such as graphene or graphite oxides. The results also demonstrate that the main diffraction peaks of pure anatase-TiO<sub>2</sub> and TiO<sub>2</sub>/C films are similar.

The comparison of G-band Raman spectra of EG nanosheets before (Figure 7(a)) and after the deposition on the TiO<sub>2</sub> film's surface (Figure 7(b)) showed that, for graphite, the G-band peak is symmetric and can be fitted with a single Gaussian curve at 1578 cm<sup>-1</sup>. Nevertheless, the G-band after the graphite deposition on TiO<sub>2</sub> two displaced peaks at 1569 and 1607 cm<sup>-1</sup> can be seen. According to the first-order Raman process [47], the results suggest that the two phonon energies of the

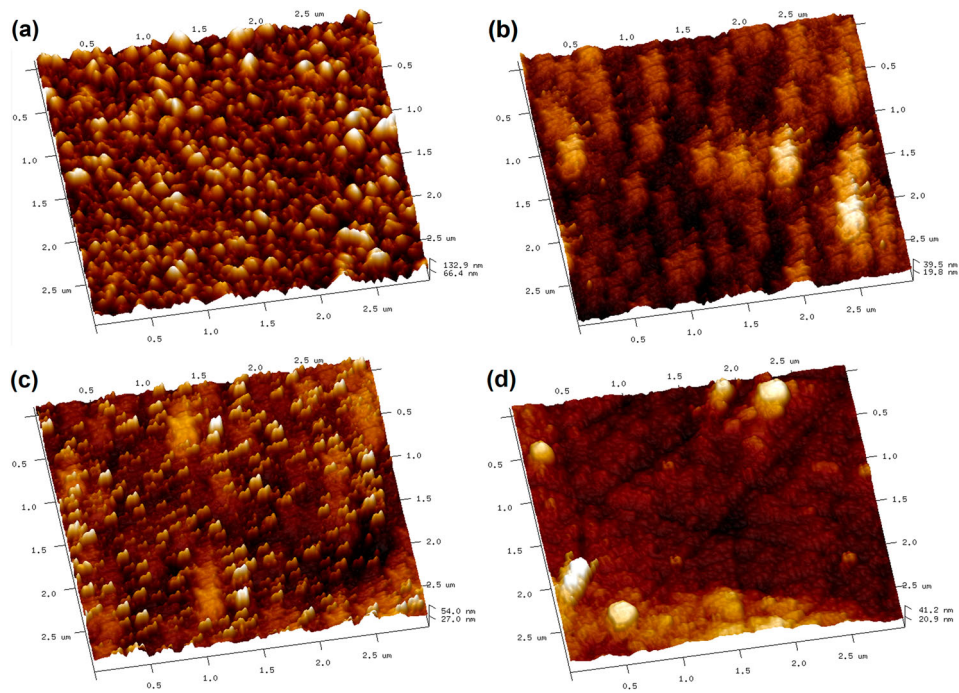


**Figure 5.** Surface AFM images of the (a)  $\text{TiO}_2$  film, and  $\text{TiO}_2/\text{C}$  decorated films at different exfoliated graphite time (b) 2 h, (c) 8 h, and (d) 24 h. The anatase- $\text{TiO}_2$  films were synthesized by sol-gel technique, deposited on borosilicate glass substrates by a facile airbrush spray coating method at room temperature, and heat treated at  $550^\circ\text{C}$ . Then, the films were coated with EG nanosheets by spray coating at room temperature, and heat treated at  $100^\circ\text{C}$ .

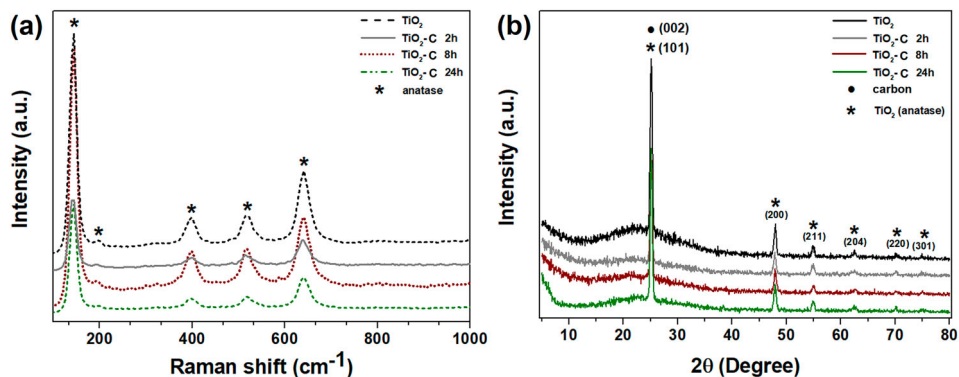
interaction between  $\text{TiO}_2$  and carbon nanosheets promoted changes of electron density distribution of the graphite – electron( $e^-$ )/hole ( $h^+$ ) p-doping observed in G-band splitting – which may have induced the  $\text{TiO}_2/\text{C}$  heterojunction formation, and consequently extended the light absorption range of photocatalyst to visible light [44,47,48].

Figure 8 describes the variation between  $(\text{ah}\nu)^{1/2}$  and the photon energy, in eV, used to estimate the band gap energies of the anatase- $\text{TiO}_2$  film and the heterostructured  $\text{TiO}_2/\text{C}$  nanocomposite films. The value of 3.23 eV found for the pure  $\text{TiO}_2$  film is reported in the literature for the anatase phase [49]. In the presence of expanded

graphite, it was observed that the  $E_g$  values reduced to approximately 3 eV. The results suggest that the addition of carbon effectively promoted the formation of the C-semiconductor heterojunction, as observed in the Raman spectroscopy results (Figure 7(b)), providing structural alterations that favoured the reduction of the  $E_g$ , and consequent absorption of lower energy photons to activate the photocatalyst under visible light.

### 3.3. Dye removal photocatalytic efficiency

Figure 9(a) shows the efficiency of  $\text{TiO}_2$  and  $\text{TiO}_2/\text{C}$  films in the photocatalytic removal of MO dye under visible



**Figure 6.** (a) Raman spectra and of the  $\text{TiO}_2$  and  $\text{TiO}_2/\text{C}$  films, (b) XRD patterns of the  $\text{TiO}_2$  and  $\text{TiO}_2/\text{C}$  films obtained by spray coating at  $550^\circ\text{C}$ .

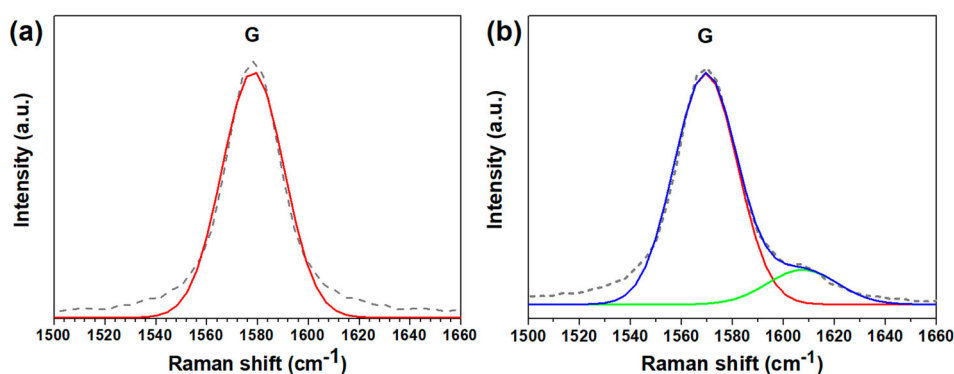


**Figure 7.** G-bands of Raman spectra of graphite. (a) before and (b) after the TiO<sub>2</sub>/C heterojunction formation.

light irradiation. The dye solution was left in the dark for 60 min to reach the equilibrium between the desorption of dye molecules and the ionic adsorption on the films. The increase in the adsorption capacity of the heterojunctions after 20 min, followed by its saturation, can be attributed to the increase in the specific surface area of the films from the carbon addition [43,44].

The MO photolysis curve shows that, without the presence of the photocatalyst, there was no dye removal under visible light. The pure anatase-TiO<sub>2</sub> film did not exhibit photoactivity under the same conditions, which agrees with results of other studies [5,9]. The measurements also suggest that the dye did not sensitize the film surface – an important condition for its practical use in photocatalytic applications. Previous studies show that the films have good stability, without presenting structural changes or delamination with their use [7,23].

The results demonstrate that the photocatalytic activity of films improved considerably under visible light due to the formation of the TiO<sub>2</sub>/C heterojunction.

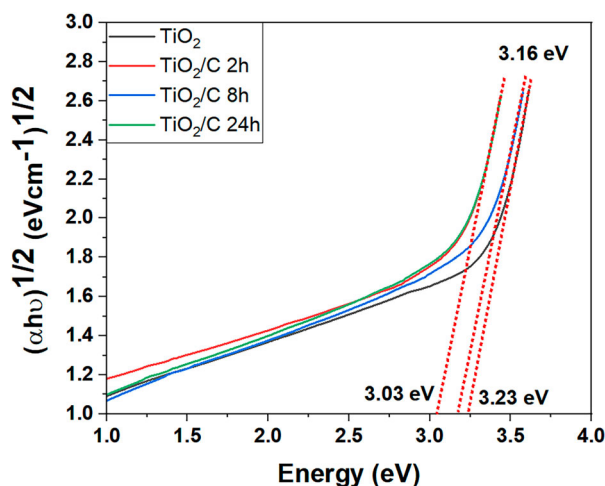


**Figure 8.** Band gap energy measurements of TiO<sub>2</sub> and TiO<sub>2</sub>/C films estimated using the Tauc method.

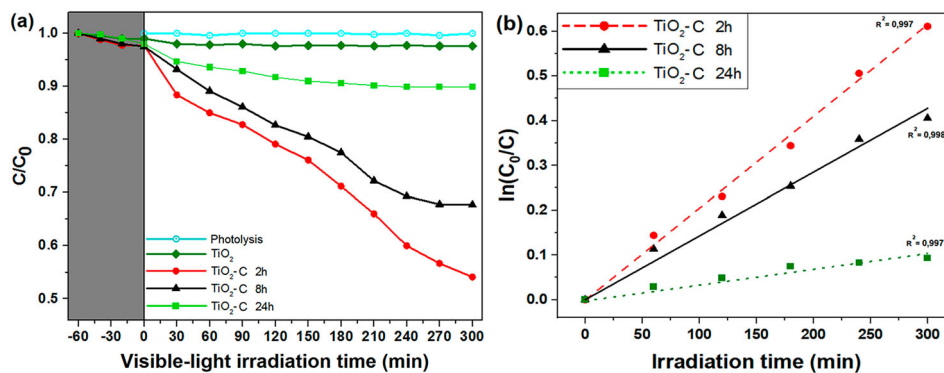
After 300 min of irradiation, approximately 49% of the MO dye was removed from the water by employing the TiO<sub>2</sub>/C film. The photocatalytic efficiency can be influenced by several factors. Such superficial modification can be observed in the morphological AFM results.

Figure 9(b) shows the kinetic curves from which the rate constants ( $k_{ap}$ ) values for the TiO<sub>2</sub>/C hybrid films were estimated. The increase in the  $k_{ap}$  value from  $6.35 \times 10^{-5} \text{ min}^{-1}$ , corresponding to the film coated with EG exfoliated in 24 h, to  $6.18 \times 10^{-4} \text{ min}^{-1}$ , referring to the film coated with EG exfoliated in 2 h – indicates an increase in the dye removal rate under visible light with a reduction in the exfoliation time of C.

It was observed that the EG that best activated the photocatalytic properties of TiO<sub>2</sub> was the one exfoliated by 2 h. The decorated-films using EG obtained for 8 and 24 h exhibited efficiency of 34% and 10%, respectively. This behaviour suggests that the photocatalytic activity of decorated films is strongly dependent on the synthesis time. The longer the exfoliation time and consequent exposure to UVC light, the lower the concentration of oxygenated groups present between the layers of the graphite, as shown in FT-IR and XPS results. The photocatalysts performance may indicate that the presence of these oxygenated functional groups – such as hydroxyls, carboxyls, carbonyls and epoxies – can promote the efficient formation of highly active radicals (O<sub>2</sub><sup>•-</sup>, HO<sup>•</sup>), contributing to the improvement of the photocatalytic activity of TiO<sub>2</sub> [15,17,50].

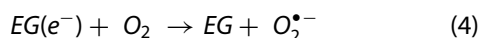
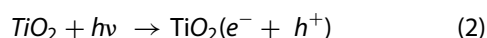
TiO<sub>2</sub> have a band gap value of 3.2 eV (Figure 8) [3,10]. The work function of exfoliated carbon at 4.5 eV promotes the maximum harvesting of sunlight and acts as an electron shuttle [44,45] – thus improving the photocatalytic behaviour of the composite and reducing the charge recombination rate.

High adsorption of contaminants, wide range of light absorption, and photogenerated charge separation are



**Figure 9.** (a) Photocatalytic decolorization of methyl orange dye (MO) by  $TiO_2$  and  $TiO_2/C$  films under visible light irradiation. The pollutant model reaction medium is MO in deionized water, concentration of  $0.005 \text{ mg L}^{-1}$ ,  $\text{pH} = 2$ .  $C_0$  is the initial concentration of MO in water, and  $C$  is the concentration after  $t$  min. All samples were heat treated at  $550^\circ\text{C}$ . As highlighted on the graph, the films and dye solution were remained into the dark for 60 min to achieve the adsorption-desorption equilibrium of the dye molecules on the photocatalyst surface; (b) Pseudo-first order kinetic curves of  $TiO_2/C$  films for dye removal under visible light.

important parameters to define high photocatalytic activity [1,7,10]. EG nanosheets can promote the efficient charge separation, restrict the electron-hole pairs recombination, and increase the specific surface area, which results in increased photocatalytic activity. In the  $TiO_2/C$  heterojunction, when the photocatalyst is illuminated by visible light, electrons ( $e^-$ ) are excited from the valence band (VB) of  $TiO_2$  to the conduction band (CB), forming electron-hole pairs: responsible for the photocatalytic activity [45,47,51]. Then, the photo-generated electron ( $e^-$ ) tends to be transferred from  $TiO_2$  to EG nanosheets, and thus eliminated by dissolved oxygen, which facilitates the charges separation [17,44]. Oxygen vacancies are formed into the photocatalyst, promoting new energy levels, and displacement of the absorption band gap to longer wavelengths [18,43,46]. The photocatalytic reaction steps in a  $TiO_2/C$  heterojunction mechanism can be expressed as shown below:



The results suggest the promising character of  $TiO_2/C$  nanostructured heterojunctions for practical photocatalytic applications. The airbrush spray coating technique showed to be efficient for the synthesis of films, which exhibited good dye removal values under visible light – favourable for its practical use in the treatment and purification of water under sunlight.

#### 4. Conclusions

Expanded graphite (EG) nanosheets were obtained by UVC-assisted liquid-phase exfoliation method. EG nanosheets were synthesized directly from graphite bulk. The results suggest that the proposed technique is a promising method to produce exfoliated carbon with high crystallinity, good thermal stability, low cost, simplicity of materials and equipment, without any addition of acids, surfactants, or aggressive oxidizing agents, which characterizes the process as an eco-friendly method.  $TiO_2$  films were obtained by sol-gel process and deposited on borosilicate glass by spray coating technique at room temperature. The films were heat treated at  $550^\circ\text{C}$ . All films presented only anatase phase. When the EG nanosheets are deposited on  $TiO_2$  films surface they promoted morphological modifications, changes in the electronic structure, and the  $TiO_2/C$  heterojunction formation – which improved the photocatalytic activity under visible light. The comparison of the G-band Raman spectra of the EG nanosheets before and after the junction with  $TiO_2$  suggests the interaction between the materials, which promoted the formation of the semiconductor-C heterojunction and favoured the reduction of the photocatalyst band gap energy by 3.2 to 3.0 eV. The results of the methyl orange dye removal showed that the  $TiO_2/C$  composite films present good photocatalytic behaviour, with an efficiency around 49%. This efficiency is strongly dependent on the EG UVC-assisted exfoliation time. The analysis of the influence of graphite exfoliation time on the photocatalytic activity of the nanocomposite films indicated the existence of an ideal time in which the hybrid photocatalyst exhibits better photocatalytic performance: 2 h of graphite exfoliation. This effect may be associated with the greater presence of

oxygenated groups. Hybrid TiO<sub>2</sub>/C supported photocatalysts obtained by spray coating are a promising alternative for practical photocatalytic applications in the water treatment under sunlight. Future plans aim to study the reuse and durability of TiO<sub>2</sub>/C nanocomposite films after several photocatalytic cycles under visible light, and evaluate the effect of reactive species on the photocatalytic performance from the use of scavengers.

## Acknowledgements

The authors are grateful to CNPq (National Council for Scientific and Technological Development, Proc. 168935/2018-0) Brazilian agency for the financial support, and the Polytechnic School of the University of São Paulo (Electrical Engineering School of POLI-USP) for the Raman spectroscopy and UV-vis spectrophotometry facility.

## Disclosure statement

No potential conflict of interest was reported by the author(s).

## Funding

This work was supported by CNPQ [grant number 168935/2018-0].

## Data availability statement

All data generated or analysed during this study are included in this published article (and its supplementary information files), and are available from the corresponding author on reasonable request.

## ORCID

Rodrigo Teixeira Bento  <http://orcid.org/0000-0002-1797-9652>

## References

- [1] Li X, Shen R, Ma S, et al. Graphene-based heterojunction photocatalysts. *Appl Surf Sci.* 2018;430:53–107. doi:10.1016/j.apsusc.2017.08.194.
- [2] Khaoulani S, Chaker H, Cadet C, et al. Wastewater treatment by cyclodextrin polymers and noble metal/mesoporous TiO<sub>2</sub> photocatalysts. *C R Chim.* 2015;18:23–31. doi:10.1016/j.crci.2014.07.004.
- [3] Reza KM, Kurny ASW, Gulshan F. Parameters affecting the photocatalytic degradation of dyes using TiO<sub>2</sub>: a review. *Appl Water Sci.* 2017;7:1569–1578. doi:10.1007/s13201-015-0367-y.
- [4] Du X, Zhou M. Strategies to enhance catalytic performance of metal-organic frameworks in sulfate radical-based advanced oxidation processes for organic pollutants removal. *Chem Eng J.* 2021;403:126346. doi:10.1016/j.cej.2020.126346.
- [5] Bento RT, Correa OV, Marina MF. Photocatalytic activity of undoped and sulfur-doped TiO<sub>2</sub> films grown by MOCVD for water treatment under visible light. *J Europ Ceram Soc.* 2019;39:3498–3504. doi:10.1016/j.jeurceramsoc.2019.02.046.
- [6] Kim K, Kim HS, Lee H. Revealing the improved catalytic properties of modified graphene-like structures. *Sci Rep.* 2020;10:2119. doi:10.1038/s41598-020-59130-z.
- [7] Marcello BA, Correa OV, Bento RT, et al. Effect of growth parameters on the photocatalytic performance of TiO<sub>2</sub> films prepared by MOCVD. *J Braz Chem Soc.* 2020;31:1270–1283. doi:10.21577/0103-5053.20200012.
- [8] Jia C, Zhang X, Yang P. Construction of anatase/rutile TiO<sub>2</sub> hollow boxes for highly efficient photocatalytic performance. *Appl Surf Sci.* 2018;430:457–465. doi:10.1016/j.apsusc.2017.06.163.
- [9] Bento RT, Correa OV, Antunes RA, et al. Surface properties enhancement by sulfur-doping on TiO<sub>2</sub> films. *Mater Res Bull.* 2021;143:111460. doi:10.1016/j.materresbull.2021.111460.
- [10] Hanaor DAH, Sorrell CC. Review of the anatase to rutile phase transformation. *J Mater Sci.* 2011;46:855–874. doi:10.1007/s10853-010-5113-0.
- [11] Duc La D, Rananaware A, Nguyen Thi HP, et al. Fabrication of a TiO<sub>2</sub>@porphyrin nanofiber hybrid material: a highly efficient photocatalyst under simulated sunlight irradiation. *Adv Nat Sci.: Nanosci Nanotechnol.* 2017;8:015009. doi:10.1088/2043-6254/aa597e. (8pp).
- [12] Xiong S, Yu Y, Wang P, et al. Growth of AgBr/Ag<sub>3</sub>PO<sub>4</sub> heterojunction on chitosan fibers for degrading organic pollutants. *Adv Fiber Mater.* 2020;2:246–255. doi:10.1007/s42765-020-00042-y.
- [13] Duoerkun G, Zhang Y, Shi Z, et al. Construction of n-TiO<sub>2</sub>/p-Ag<sub>2</sub>O junction on carbon fiber cloth with Vis-NIR photoresponse as a filter-membrane-shaped photocatalyst. *Adv Fiber Mater.* 2020;2:13–23. doi:10.1007/s42765-019-00025-8.
- [14] Sun Y, Mwandeje JB, Wangatia LM, et al. Enhanced photocatalytic performance of surface-modified TiO<sub>2</sub> nanofibers with Rhodizonic acid. *Adv Fiber Mater.* 2020;2:118–122. doi:10.1007/s42765-020-00037-9.
- [15] Tang B, Chen H, Peng H, et al. Graphene modified TiO<sub>2</sub> composite photocatalysts: mechanism, progress and perspective. *Nanomaterials.* 2018;8(2):105. doi:10.3390/nano8020105.
- [16] Xiang QJ, Yu JG, Jaroniec M. Graphene-based semiconductor photocatalysts. *Chem Soc Rev.* 2012;41:782–796. doi:10.1039/C1CS15172J.
- [17] Khalid NR, Bilal Tahir M, Majid A, et al. TiO<sub>2</sub>-graphene-based composites: synthesis, characterization, and application in photocatalysis of organic pollutants. *Micro Nanomanufact.* 2018;2:95–122. doi:10.1007/978-3-319-67132-1\_5.
- [18] Wu F, Liu W, Qiu J, et al. Enhanced photocatalytic degradation and adsorption of methylene blue via TiO<sub>2</sub> nanocrystals supported on graphene-like bamboo charcoal. *Appl Surf Sci.* 2015;358:425–435. doi:10.1016/j.apsusc.2015.08.161.
- [19] Jia J, Li D, Wan J, et al. Characterization and mechanism analysis of graphite/C-doped TiO<sub>2</sub> composite for enhanced photocatalytic performance. *J Ind Eng Chem.* 2016;33:162–169. doi:10.1016/j.jiec.2015.09.030.

- [20] Jiang B, Tian C, Zhou W, et al. In situ growth of TiO<sub>2</sub> in interlayers of expanded graphite for the fabrication of TiO<sub>2</sub>-graphene with enhanced photocatalytic activity. *Chem Europ J.* 2011;17:8379–8387. doi:10.1002/chem.201100250.
- [21] Zhang J, Wang X, Wang X, et al. Floating photocatalysts based on loading Bi/N-doped TiO<sub>2</sub> on expanded graphite C/C (EGC) composites for the visible light degradation of diesel. *RSC Adv.* 2015;5:71922–71931. doi:10.1039/C5RA12783A.
- [22] Murugan C, Ranjithkumar K, Pandikumar A. Interfacial charge dynamics in type-II heterostructured sulfur doped-graphitic carbon nitride/bismuth tungstate as competent photoelectrocatalytic water splitting photoanode. *J Colloid Interf Sci.* 2021;602:437–451. doi:10.1016/j.jcis.2021.05.179.
- [23] Bento RT, Correa OV, Pillis MF. On the surface chemistry and the reuse of sulfur-doped TiO<sub>2</sub> films as photocatalysts. *Mater Chem Phys.* 2021;261:124231. doi:10.1016/j.matchemphys.2021.124231.
- [24] De Oliveira EC, Bento RT, Correa OV, et al. Visible-light photocatalytic activity and recyclability of N-doped TiO<sub>2</sub> films grown by MOCVD. *Cerâmica.* 2020;66(380):451–459. doi:10.1590/0366-69132020663802957.
- [25] Peng L, Xu Z, Liu Z, et al. An iron-based green approach to 1-h production of single-layer graphene oxide. *Nat Commun.* 2015;6:5716. doi:10.1038/ncomms6716.
- [26] Swain KA, Bahadur D. Enhanced stability of reduced graphene oxide colloid using cross-linking polymers. *J Phys Chem C.* 2014;118:9450–9457. doi:10.1021/jp500205n.
- [27] Xue B, Zou Y, Yang Y. A UV-light induced photochemical method for graphene oxide reduction. *J Mater Sci.* 2017;52:12742–12750. doi:10.1007/s10853-017-1266-4.
- [28] Mozumder A, Magee JL. Model of tracks of ionizing radiation for radical reaction mechanisms. *Radiat Res.* 1966;28:203–214. doi:10.2307/3572190.
- [29] Ji T, Hua Y, Sun M, et al. The mechanism of the reaction of graphite oxide to reduced graphene oxide under ultraviolet irradiation. *Carbon N Y.* 2013;54:412–418. doi:10.1016/j.carbon.2012.11.057.
- [30] Yin R, Shen P, Lu Z. A green approach for the reduction of graphene oxide by ultraviolet/sulfite process. *J Colloid Interf Sci.* 2019;550:110–116. doi:10.1016/j.jcis.2019.04.073.
- [31] Bera M, Pragya Gupta C, Maji PK. Facile one-pot synthesis of graphene oxide by sonication assisted mechanochemical approach and its surface chemistry. *J Nanosci Nanotechnol.* 2018;18:902–912. doi:10.1166/jnn.2018.14306.
- [32] Ruiz S, Tamayo JA, Ospina JD, et al. Antimicrobial films based on nanocomposites of chitosan/poly(vinyl alcohol)/graphene oxide for biomedical applications. *Biomolecules.* 2019;9(3):109. doi:10.3390/biom9030109.
- [33] Verma S, Dutta RK. A facile method of synthesizing ammonia modified graphene oxide for efficient removal of uranyl ions from aqueous medium. *RSC Adv.* 2015;5(94):77192–77203. doi:10.1039/c5ra10555b.
- [34] Freitas LV, Lima KCMS, Silva SM, et al. Amperometric electrochemical platform for hydrazine determination exploiting reduced graphene oxide: co(salophen) and DNA: application in pharmaceutical formulations samples. *J Braz Chem Soc.* 2018;29(10):2096–2103. doi:10.21577/0103-5053.20180084.
- [35] Eigler S, Dotzer C, Hirsch A, et al. Formation and decomposition of CO<sub>2</sub> intercalated graphene oxide. *Chem Mater.* 2012;24(7):1276–1282. doi:10.1021/cm203223z.
- [36] Nam PT, Khanh NV, Thom NT, et al. Synthesis of reduced graphene oxide for high-performance supercapacitor. *Vietnam J Chem.* 2018;56(6):778–785. doi:10.1002/vjch.201800087.
- [37] Guerrero-Contreras J, Caballero-Briones F. Graphene oxide powders with different oxidation degree; prepared by synthesis variations of the Hummers method. *Mater Chem Phys.* 2015;153:209–220. doi:10.1016/j.matchemphys.2015.01.005.
- [38] Wei L, Chen F, Wang H, et al. Acetone-induced graphene oxide film formation at the water-air interface. *Chem Asian J.* 2013;8:437–443. doi:10.1002/asia.201200921.
- [39] Rui B, Yang M, Zhang L, et al. Reduced graphene oxide-modified biochar electrodes via electrophoretic deposition with high rate capability for supercapacitors. *J App Electrochem.* 2020;50:407–420. doi:10.1007/s10800-020-01397.
- [40] Diez N, Sliwak A, Gryglewicz S, et al. Enhanced reduction of graphene oxide by high-pressure hydrothermal treatment. *RSC Adv.* 2015;5:81831–81837. doi:10.1039/c5ra14461b.
- [41] Xue B, Zou Y, Yang Y. UV-assisted reduction of graphite oxide to graphene by using a photoinitiator. *J Mater Sci.* 2017;52:4866–4877. doi:10.1007/s10853-016-0721-y.
- [42] Tang H, Gao P, Bao Z, et al. Conductive resilient graphene aerogel via magnesio-thermic reduction of graphene oxide assemblies. *Nano Res.* 2015;8:1710–1717. doi:10.1007/s12274-014-0671-z.
- [43] Liu P, Liu J, Zhang B, et al. Enhanced electroluminescent performance by doping organic conjugated ionic compound into graphene oxide hole-injecting layer. *J Mater Sci.* 2019;54:12688–12696. doi:10.1007/s10853-019-03820-1.
- [44] Liu X, Cong R, Cao L, et al. The structure, morphology and photocatalytic activity of graphene-TiO<sub>2</sub> multilayer films and charge transfer at the interface. *New J Chem.* 2014;38:2362–2367. doi:10.1039/C3NJ01003A.
- [45] Zabihi F, Ahmadian-Yazdi M-R, Eslamian M. Photocatalytic graphene-TiO<sub>2</sub> thin films fabricated by low-temperature ultrasonic vibration-assisted spin and spray coating in a sol-gel process. *Catalysts.* 2017;7:136. doi:10.3390/catal7050136.
- [46] Tismanar I, Obreja AC, Buiu O, et al. VIS-active TiO<sub>2</sub>-graphene oxide composite thin films for photocatalytic applications. *App Surf Sci.* 2021;538:147833. doi:10.1016/j.apsusc.2020.147833.
- [47] Dong X, Shi Y, Zhao Y, et al. Symmetry breaking of graphene monolayers by molecular decoration. *Phys Rev Lett.* 2009;102:135501. doi:10.1103/PhysRevLett.102.135501.
- [48] Lee J, Novoselov KS, Shin HS. Interaction between metal and graphene: dependence on the layer number of graphene. *ACS Nano.* 2011;5:608–612. doi:10.1021/nn103004c.
- [49] Ali T, Mohyuddin S, Ali G, et al. Synthesis of graphene doped TiO<sub>2</sub> nanotubes, and their structural, electronic,

- and photocatalytic characterization. *Electron Mater Lett.* **2022**;18:69–78. doi:[10.1007/s13391-021-00317-5](https://doi.org/10.1007/s13391-021-00317-5).
- [50] Jiang G, Lin Z, Chen C, et al.  $\text{TiO}_2$  nanoparticles assembled on graphene oxide nanosheets with high photocatalytic activity for removal of pollutants. *Carbon N Y.* **2011**;49:2693–2701. doi:[10.1016/j.carbon.2011.02.059](https://doi.org/10.1016/j.carbon.2011.02.059).
- [51] Kusiak-Nejman E, Morawski AW.  $\text{TiO}_2$ /graphene-based nanocomposites for water treatment: a brief overview of charge carrier transfer, antimicrobial and photocatalytic performance. *Appl Catal B: Environ.* **2019**;253:179–186. doi:[10.1016/j.apcatb.2019.04.055](https://doi.org/10.1016/j.apcatb.2019.04.055).